

Diode Laser-Driven Microthrusters: A New Departure for Micropropulsion

Claude Phipps*

Photonic Associates, Santa Fe, New Mexico 87505

and

James Luke†

University of New Mexico, Albuquerque, New Mexico 87106

We developed an entirely new type of orientation thruster for micro- and nanosatellites. The laser plasma thruster is based on the recent commercial availability of diode lasers with sufficient brightness and 100% duty cycle to produce a repetitively pulsed or continuous vapor or plasma jet on a surface in vacuum. A low-voltage semiconductor switch can drive the laser. A lens focuses the laser diode output on the ablation target, producing a miniature jet that provides the thrust. Single-impulse dynamic range is nearly five orders of magnitude, and the minimum impulse bit is 1 nN/s in a 100- μ s pulse. Even with diffraction-limited focusing optics, at least 0.5-W optical power is needed to produce thrust from selected ablator materials. Thrust-to-power ratio C_m is 50 to 100 μ N/W and specific impulse I_{sp} is 200–500 s with a 1-W laser, depending partially on the illumination mode. Transmission and reflection (R) illumination modes are discussed. R mode gives about 50% better I_{sp} and two times better C_m . Improved results are anticipated from higher laser power in the reflection mode. The prototype engine we are developing is intended to provide lifetime on-orbit steering for a 5-kg satellite, as well as reentering it from low Earth orbit.

Nomenclature

A	=	area of output facet
B	=	beam brightness, $\text{Wm}^{-2} \text{sterrad}^{-1}$
C_m	=	laser momentum coupling coefficient, N/W
d	=	diameter of pendulum fiber
d_s	=	diameter of laser spot on target
d_0	=	beam waist diameter (minimum laser spot diameter)
F	=	thrust, N
F_1	=	torsional pendulum force
F_2	=	calibrating pendulum force
G	=	torsion modulus of pendulum fiber
g	=	acceleration of gravity on Earth's surface (9.8 m/s^2)
I	=	moment of inertia of torsion pendulum
I_{sp}	=	specific impulse, s
J	=	polar moment of inertia of pendulum fiber
k	=	torsional spring constant
L	=	effective length of pendulum fiber
L_t	=	effective length of calibrating pendulum
M	=	initial ablatant mass
m	=	effective mass of torsion pendulum
P	=	incident laser power, W
p	=	impulse, N-s
Q^*	=	laser energy required to ablate 1 kg
R	=	effective radius of torsion pendulum
v_E	=	exhaust velocity, m/s
W	=	incident laser pulse energy
x_1	=	displacement of torsion pendulum
x_2	=	displacement of calibrating pendulum
x_{th}	=	thermal penetration depth
Δm	=	ablated mass

Δv	=	change in spacecraft velocity
θ	=	torsional pendulum deflection
θ_b	=	probe beam deflection
θ_0	=	peak pendulum deflection, rad
η_{AB}	=	ablation efficiency
κ	=	thermal diffusivity, m^2/s
τ	=	laser pulse duration, s
τ_{AB}	=	ablator lifetime
Φ	=	laser fluence, J/m^2
Φ_{opt}	=	laser fluence that produces maximum C_m
Ω	=	solid angle, steradians
ω_0	=	resonant frequency of torsion pendulum

Introduction: Need for a New Microthruster

THROUGHOUT most of the history of space propulsion, the emphasis has been on producing rocket engines with ever larger thrust. Now, with the advent of microsattelites (>10 kg), nanosatellites (1–10 kg), and even picosatellites (<1 kg) this trend is reversing in one branch of motor development. Desirable features of such an engine are thrust per axis 100 μ N; less than 1-kg dry weight; size of order $2 \times 10 \times 12$ cm; specific impulse of order 500 s; single-impulse dynamic range 10,000:1; continuous or impulsive thrust; zero off-state power; low-voltage operation; no nozzle; and inexpensive fuel materials and components.

Recent developments in high-brightness diode lasers have been dramatic. The focused intensity available with these devices suggests that a laser-diode-driven plasma jet is possible and represents a way of achieving the preceding features. Figure 1 shows how the engine would work in reflection (R) and transmission (T) mode.

We are developing a prototype engine with which we intend to demonstrate the features just listed. We have demonstrated that all of these features are individually feasible, and it is the purpose of this paper to report the results of our research program. Features we have demonstrated and report here include continuous operation, very large single-impulse dynamic range, good I_{sp} , and excellent thrust-to-power ratio. We believe that the laser plasma thruster (LPT) will prove an attractive alternative to the micropulsed plasma thruster.

Laser Diode Capabilities

Recently, high-brightness diode lasers¹ have become available with optical power up to 4 W from a single $100 \times 1 \mu\text{m}$ facet, electrical efficiency in excess of 50%, 100% duty cycle, and operating

Received 7 August 2000; revision received 10 June 2001; accepted for publication 29 June 2001. Copyright © 2001 by Photonic Associates. Published by the American Institute of Aeronautics and Astronautics, Inc., with permission. Copies of this paper may be made for personal or internal use, on condition that the copier pay the \$10.00 per-copy fee to the Copyright Clearance Center, Inc., 222 Rosewood Drive, Danvers, MA 01923; include the code 0001-1452/02 \$10.00 in correspondence with the CCC.

*President, 200A Ojo de la Vaca Road; CRPhipps@aol.com. Member AIAA.

†Research Assistant Professor, Engineering Research Institute, 901 University Boulevard, SE. Member AIAA.

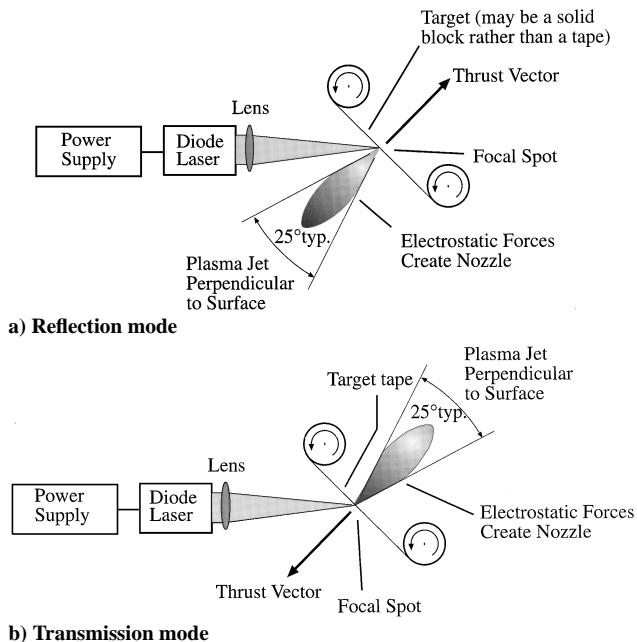


Fig. 1 Schematic diagram of the LPT, contrasting R and T modes of target illumination. R-mode advantages are improved I_{sp} and C_m , whereas T-mode advantages are protection of optics from ablation debris.

case temperature up to 95°C. Mean time between failures is 100,000 h at 40°C (Osinski, J., private communication, SDL, Inc., San Jose, CA, May 2001).

A diffraction-limited, 1-W flare-type single-transverse-mode diode at 935-nm wavelength potentially achieves brightness $B = P/\lambda^2 = 1 \text{ TWm}^{-2} \text{ sterad}^{-1}$. In practice, they can easily be focused to 5- μm -diam spots with $f/2$ optics to produce 50-GW/m² intensity on target.

Even the less-bright multi-transverse-mode diodes with emitter effective area $A = 100 \mu\text{m}^2$ [100 μm long \times one wavelength effective width] typically emit 80% of their output into $\Omega = 0.07$ steradians, giving $B = 0.8P/(A\Omega) \approx 0.5 \text{ TW m}^{-2} \text{ sterad}^{-1}$ for the 4-W Model 6380-A device made by SDL, Inc. (Osinski, private communication). In practice, these can readily be focused with 0.65 NA (numerical aperture) [less than $f/1$] optics to produce a 400–500- μm^2 spot, giving 10 GW/m² on target. As we will show, these intensities are sufficient to form plasma on absorbing materials. Diodes are constant-power (nonstorage) devices.

Plasma Formation with Diodes

Laser ablation² is the process by which a laser heats a solid surface sufficiently to eject atoms from the surface. This process is complex, covers a wide range of parameters and can involve “phase explosion,”³ as well as vapor production and plasma formation in the vapor immediately above the surface.

Laser impulse production by pulsed-laser-induced ablation in vacuum is well understood.^{4,5} The maximum momentum per joule of incident laser light is produced at a fluence Φ_{opt} , which is at or just beyond the threshold for plasma formation, because plasma inhibits coupling. Even with laser spot size d_s as small as 5 μm , impulse coupling efficiency C_m and the fluence Φ_{opt} at which it occurs are well-predicted. Apart from slowly varying factors related to dimensionality of the expansion and the ratio of d_s to thermal penetration depth during the pulse, estimates based on the large existing literature for centimeter scale interactions will apply.

To estimate the fluence required to produce plasma jets on a surface, we surveyed the literature in which the fluence for optimum coupling and plasma formation were reported. These are summarized in Fig. 2 (Refs. 5–21).

Figure 2 predicts that diodes with pulse durations at least 0.2–1 ms will be able to produce plasma jets. However, for most of these data thermal diffusivity κ could be ignored, i.e., the ratio of $x_{th} = (\kappa\tau)^{1/2}$ to laser spot diameter d_s was $\ll 1$, either because

Table 1 Figure of merit for selecting target materials is the ratio x_{th}/d_s of thermal diffusion distance during 100 μs to $d_s = 5 \mu\text{m}$. The figure of merit is shown for several materials^{22–24}

Material	x_{th} (100 μs)	x_{th}/d_s
PMMA	1.1 μm	0.22
Polyvinylchloride	3.1 μm	0.62
Silica	9.2 μm	1.7
Nylon	29	5.6
Carbon phenolic	40 μm	8.0
Tungsten carbide	50 μm	9.9
Aluminum	88	1.7
Copper	110 μm	21
Graphite	130 μm	25

of large spots, short pulses, or both. Table 1 (Refs. 22–24) gives this ratio for several materials and indicates that 2–20 times greater fluence than the Fig. 2 values will be required to compensate thermal conductance with our very small spots and relatively long pulses in highly conductive materials where the figure of merit $x_{th}/d_s \geq 1$. This is what we found.

For example, we were not able to produce a spark on aluminum. With 1-W laser power in our research setup (0.66 W actually delivered to the surface), it was necessary to use ablatants with low thermal conductivity such as polyvinylchloride (PVC).

Laser Impulse Coupling Physics

The momentum coupling coefficient C_m is defined as the ratio of target momentum $m\Delta v$ produced to incident laser pulse energy W during the ejection of laser-ablated material (the photoablation process). For continuous lasers it is the ratio of thrust F to incident power P :

$$C_m = m\Delta v/W = F/P \quad (1)$$

In the ablation process Q^* joules of laser light (the asterisk is customary notation: Q^* is not a complex number) are consumed to ablate each gram of target material:

$$Q^* = W/\Delta m \quad (2)$$

For the sake of discussion, we will consider a monoenergetic exhaust stream with velocity v_E . Momentum conservation requires

$$m\Delta v = \Delta m v_E \quad (3)$$

so that the product of C_m and Q^* is the effective exhaust velocity v_E of the laser rocket, independent of the efficiency with which laser energy is absorbed. This can be seen by writing

$$C_m Q^* = \frac{(N-s)(J)}{(J)(\text{kg})} = \frac{(\text{kg})(\text{m})}{(\text{kg})(\text{s})} = \text{m/s} \quad (4)$$

If, for example, a significant amount of the incident energy is absorbed as heat in the target substrate rather than producing material ejection, Q^* will be higher, and C_m will be proportionately lower, giving the same velocity in the end.

Although it is understood that real exhaust streams have velocity distributions, we have shown²⁵ that the monoenergetic stream approximation will not introduce large errors ($\langle v^2 \rangle / \langle v \rangle^2 \approx 1.15$) for laser-produced plasmas, and the principal points we want to make will be easier to understand using that assumption.

The specific impulse I_{sp} is simply related to the velocity v_E by the acceleration of gravity:

$$C_m Q^* = v_E = g I_{sp} \quad (5)$$

Energy conservation prevents C_m and Q^* from being arbitrary. Increasing one decreases the other. Using Eqs. (1) and (2), energy conservation requires that several constant product relationships exist:

$$2\eta_{AB} = \Delta m v_E^2 / W = C_m^2 Q^* = g C_m I_{sp} = C_m v_E \quad (6)$$

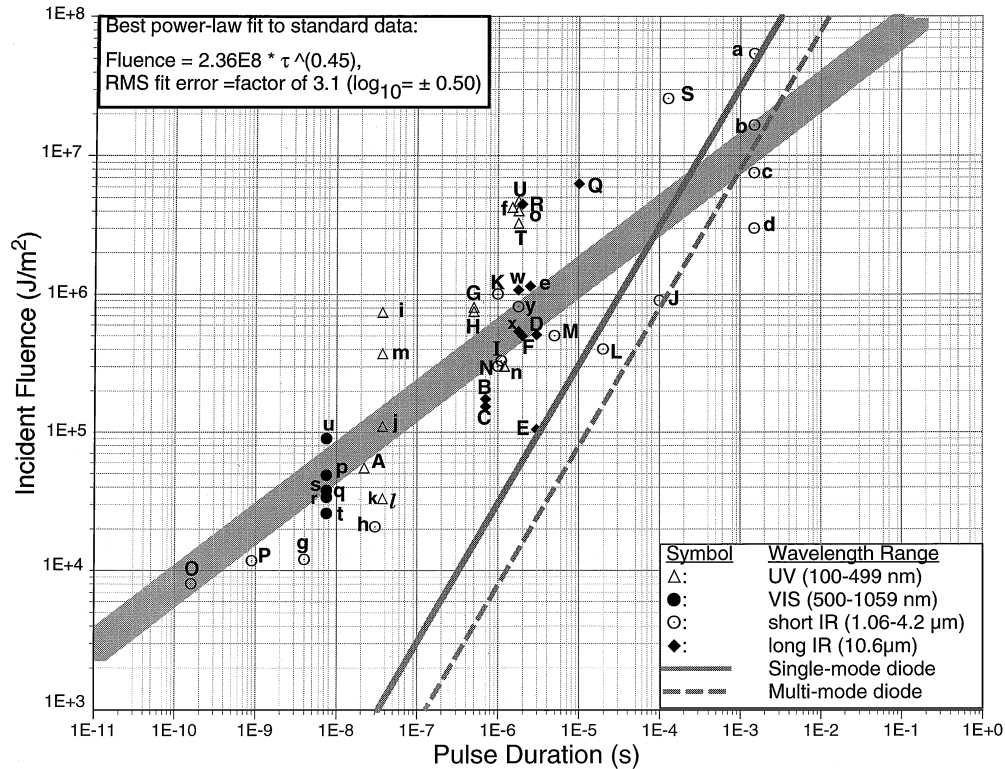


Fig. 2 Fluence required to be incident on the target vs pulse duration for peak coupling and plasma formation from 46 data sets reported in the literature for which peak coupling was recorded. The broad gray bar $\Phi = A\tau^B$ with $A = 2.38E4$ and $B = 0.45$ represents the best fit to the data. Thermal theory gives $B = 0.50$. Wavelengths for the data are indicated in the box in the lower-right-hand corner. The solid gray line is the fluence produced by a 0.66-W, single-transverse-mode diode with 5- μm spot size. The dashed gray line is fluence produced by a 4-W multimode diode imaged to a $5 \times 100 \mu\text{m}$ spot on target using fast aspheric optics. The indication is that either one can produce a plasma and achieve Φ_{opt} with pulses longer than 0.2–1 ms. The minority of experiments reported in the literature for which the peak momentum coupling fluence Φ_{opt} was measured or can be deduced give the 46 data points shown. Representing lasers with wavelength from 248 nm to 10.6 μm and pulse durations 300 fs $< \tau < 1$ ms acting on metals and nonmetals, they follow a trend (the gray bar) to within an rms fit error of a factor of 3 at any given pulse duration. References corresponding to the points are as follows: a, b, c, d: aluminum, copper, graphite, and lead, Ref. 6; e: bismuth, Ref. 7; f: aluminum, Ref. 8; g, h, O, P: aluminum, Ref. 9; i, k, l, m: tantalum, titanium, PMMA, and aluminum (see Ref. 10, pp. 213–234); n: aluminum, Ref. 11; o: aluminum (see Ref. 10, pp. 211, 212); p, q, r, s, t, u: beryllium, graphite, aluminum, zinc, silver, and tungsten, Ref. 12; w, x, A: aluminum, kevlar epoxy, and nylon, Ref. 5; y: kevlar epoxy (see Ref. 10); z: copper, Ref. 13; B, C: cellulose acetate, Ref. 14; E, F: carbon phenolic and graphite, Ref. 15; G: titanium, Ref. 16; H: aluminum, Ref. 17; I, J, K, L, M: titanium and grafoil, Ref. 18; Q: aluminum, Ref. 19; R: stainless steel, Ref. 20; S: aluminum, Ref. 21; and T, U: aluminum (see Ref. 10, pp. 199–202).

In Eq. (6) we introduce the ablation efficiency parameter $\eta_{\text{AB}} \leq 1$, the efficiency with which laser energy W is converted into exhaust kinetic energy. Choosing combinations of C_m and v_E that exceed 2 violates physics because η_{AB} must be less than 1.

Because the maximum specific impulse of ordinary chemical rockets is about 500 s, limited by the temperatures available in chemical reactions, exit velocity $v_E > 5$ km/s ($I_{\text{sp}} > 500$ s) is accessible only by laser ablation or some other nonchemical process such as ion drives.

Ablation efficiency can approach 100%, as direct measurements with other types of lasers on cellulose nitrate in vacuum verify,⁵ but a value of 50% or even less is likely. The impact of $\eta_{\text{AB}} < 1$ is that the C_m value deduced from a given v_E might be less than the maximum permitted by conservation of energy. Exit velocity v_E is the fundamental quantity.

Some of the factors that affect ablator lifetime are shown in Eq. (7), where the final term emphasizes the crucial importance of I_{sp} :

$$\tau_{\text{AB}} = |M/\dot{m}| = MgI_{\text{sp}}/F \quad (7)$$

In Eq. (7) M is the initial ablatant mass, and \dot{m} is the mass ablation rate. The vacuum coupling coefficient C_m is in the range 10–100 $\mu\text{N}/\text{W}$ for many standard surface-absorbing materials.⁴

Experiments

Purpose

The purpose of our research program was to determine what materials give good I_{sp} and suitable C_m for a microthruster when illuminated by focused laser diodes.

Torsion Balance

To measure impulses five orders of magnitude upward from nano-Newtons/second, we constructed a highly sensitive torsion pendulum (Figs. 3 and 4). Although this fact is not specifically relevant to our measurement program, the sensitivity of the pendulum is illustrated by the fact that it readily responded to the pressure (not ablation pressure) of 1 W of laser light.

Torsion Balance Operation

The pendulum deflection θ is evaluated by reflecting a probe laser off a micromirror mounted to the center of the torsion mechanism (Fig. 3), and pendulum rotation

$$\theta = \theta_b/2 \quad (8)$$

is half the probe beam deflection (Fig. 5). The method for measuring θ_b is discussed in the section “Experimental Setup.” Torque M defines the constant k :

$$M = FR = k\theta \quad (9)$$

$$k = GJ/L \quad (10)$$

$$1/L = 1/L_1 + 1/L_2 \quad (11)$$

$$J = \pi d^4/32 \quad (12)$$

Equating kinetic and stored energy

$$W = k\theta_0^2/2 = p^2/2m = I\omega_0^2\theta_0^2/2 \quad (13)$$

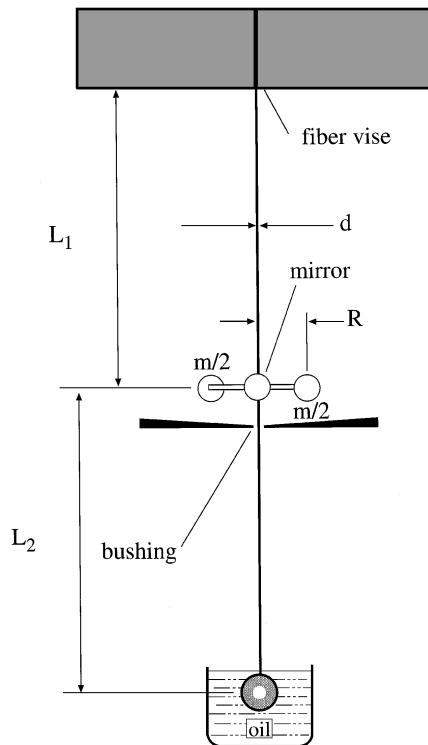


Fig. 3 Two torsion balances were constructed from $d = 78 \mu\text{m}$ fused silica fiber to make coarse and fine measurements. These differed mainly in the magnitude of the rotating mass. $L_1 \approx L_2 \approx 10 \text{ cm}$. Either position labeled $m/2$ is equivalent for mounting the target. For the light pendulum the rotating effective mass was 17.3 mg (see Table 3). The fiber vise is attached to a stepper motor and 200:1 gearbox, which rotates it in $300\text{-}\mu\text{rad}$ steps for precise positioning of the target. Target position is maintained within $\pm 3 \mu\text{m}$ for weeks.

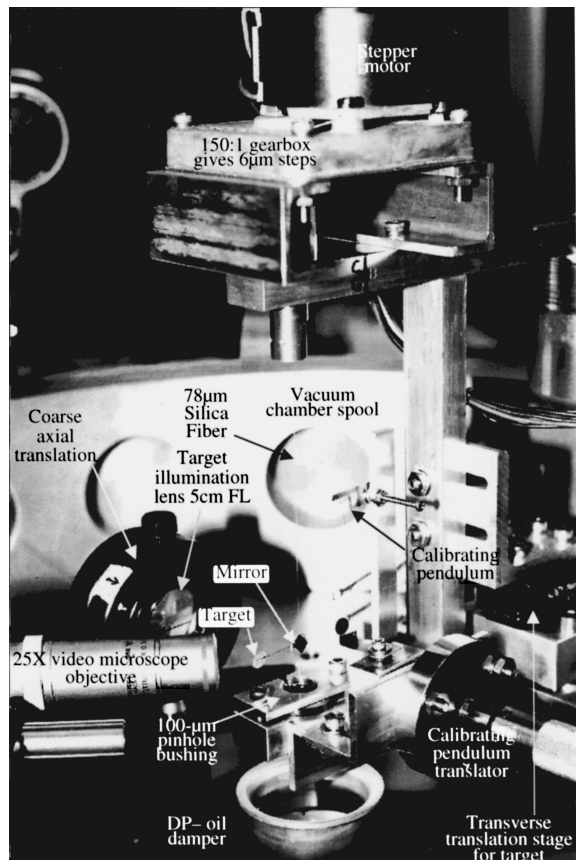


Fig. 4 Torsion pendulum under calibration.

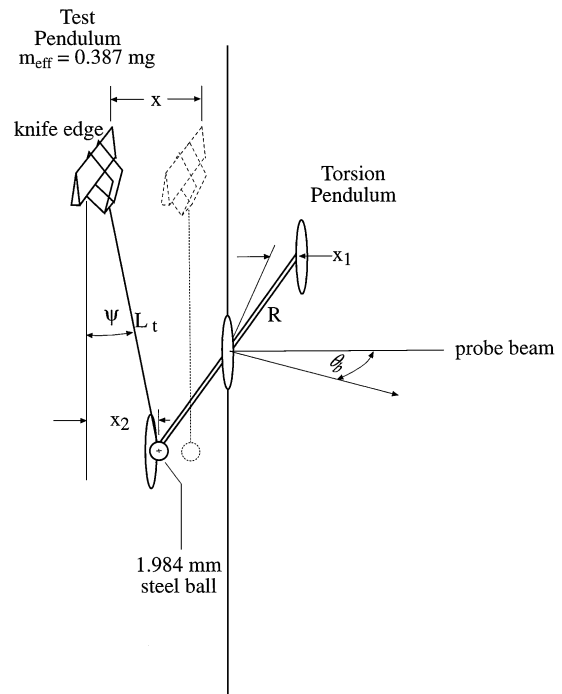


Fig. 5 Force calibration was found to be much more accurate than impact calibration.

gives the resonant frequency

$$\omega_0 = \sqrt{k/I} \quad (14)$$

In the preceding

$$I = mR^2 \quad (15)$$

θ_0 is pendulum peak deflection in response to impulse p . From Eq. (13) the impulse response of the pendulum is

$$p/\theta_0 = \sqrt{km} = \sqrt{GJm/L} = \sqrt{(\pi Gm/32L)d^2} \quad (16)$$

and the force response

$$F/\theta = GJ/LR = (\pi G/32LR)d^4 \quad (17)$$

Torsion Balance Calibration

These relationships suggest four distinct ways of determining the value of the product GJ by calibration or direct calculation: From Eq. (14) by observing the resonant frequency of the pendulum and calculating the effective rotating mass,

$$(GJ)_1 = LmR^2\omega_0^2 \quad (18)$$

or, by direct calculation based on tabulated material constants for our $78\text{-}\mu\text{m}$ -diam fused silica fiber,

$$(GJ)_2 = \pi d^4 G/32 = 109.0 \quad (19)$$

or, by applying a known force from a standard pendulum and observing the deflection θ ,

$$(GJ)_3 = FLR/\theta \quad (20)$$

or, by applying a known impulse p via a collision with a standard pendulum and observing the deflection amplitude,

$$(GJ)_4 = p^2 L/m\theta_0^2 \quad (21)$$

Of these, method 3 gave by far the most precise result. Method 1 was difficult to do accurately but did provide a useful way to account for varying response caused by small variations in target mass that occur from test to test after calibration. Method 2 is not a direct method. With method 4 accurately measuring the recoil was difficult, and finding materials with the correct coefficient of restitution for zero recoil of the test mass was more difficult. With method 3 the measured variables were simple and static, giving a measurement accuracy better than 5%.

Table 2 Pendulum response parameters

Pendulum	Light	Heavy
Resonant frequency, Hz	1.73	0.33
Effective mass, mg	17.3	580
L_1 , m	0.10	0.10
L_2 , m	0.070	0.10
p/θ_0 , $\mu\text{N-s/rad}$	$6.81 \pm 4\%$	$35.8 \pm 4\%$
F/θ , $\mu\text{N/rad}$	$134 \pm 4\%$	$110.4 \pm 4\%$
Resolution, pN-s	200	1000
Capacity, $\mu\text{N-s}$	$4.0 \pm 4\%$	$20 \pm 4\%$

To do the calibration, it was necessary to take account of the fact that both pendula move when the test pendulum is advanced a distance x via a micrometer stage. Because x was the measured variable, it was never necessary to measure the angle Ψ . We have

$$x = x_1 + x_2 \quad (22)$$

$$F_1 = \frac{GJ\theta \cos\theta}{LR} \approx \frac{GJx_1}{LR^2} \quad (23)$$

$$F_2 = m_{\text{eff}}g \tan\Psi \approx \frac{m_{\text{eff}}gx_2}{L_t} \quad (24)$$

$$GJ \left(\frac{LR^2}{GJ} + \frac{L_t}{m_{\text{eff}}g} \right) \approx \frac{2RLx}{\theta_b} \quad (25)$$

The approximation in Eq. (23) was accounted for by using small displacements. Friction hysteresis was accounted for by comparing measurement series with x increasing vs x decreasing and eliminating displacements large enough to cause hysteresis outside the desired measurement accuracy.

This simple method resulted in the calibration data shown Table 2. The value for $GJ = (GJ)_3$ obtained from the calibration agreed with the calculated value $(GJ)_2$ to within 1%. Given an accurate value for GJ , what is ultimately desired, of course, is the momentum coupling coefficient C_m :

$$C_m = (p/\theta_0)(\theta_0/W) \quad (26)$$

where $\theta_b = 2\theta_0$ and W are the measured quantities.

Time-Average Fluence

With the lightweight pendulum and to a much smaller extent with the heavy one, target acceleration leads to substantial target motion during the longer laser pulses. This leads to time-varying fluence, a situation we want to avoid. It was important to be able to correct data when this variation was slight, as well to indicate when it was necessary to switch to the heavy pendulum to get a meaningful measurement. Further, in about half the shots we deliberately chose $d_s \gg d_0$, say 100 μm instead of 5 μm , to obtain data for coupling for a range of fluence as well to anticipate coupling with multimode diodes. With so many variables we needed an analytical method of determining the fluence variation during a pulse.

Taking

$$\langle\Phi\rangle = \frac{1}{\tau} \int_0^\tau dt \Phi(t) = \frac{4W_L f_\#^2}{\pi\tau} \int_0^\tau \frac{dt}{d^2(t)} \quad (27)$$

$$d^2(t) = d_0^2 + \left(\sqrt{d_s^2 - d_0^2} + \frac{z}{f_\#} \right)^2 \quad (28)$$

with

$$d_1 = \sqrt{d_s^2 - d_0^2} \quad (29)$$

we have (please refer to Fig. 6)

$$\begin{aligned} \langle\Phi\rangle &= \frac{4W_L f_\#^2}{\pi\tau} \int_0^\tau \frac{dt}{(f_\#d_1 + z)^2 + (f_\#d_0)^2} \\ &= C \int_0^\tau \frac{dt}{(\alpha + \beta t^2)^2 + \gamma^2} \end{aligned} \quad (30)$$

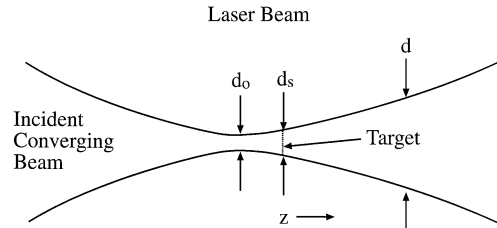


Fig. 6 Illustrating parameters near focus.

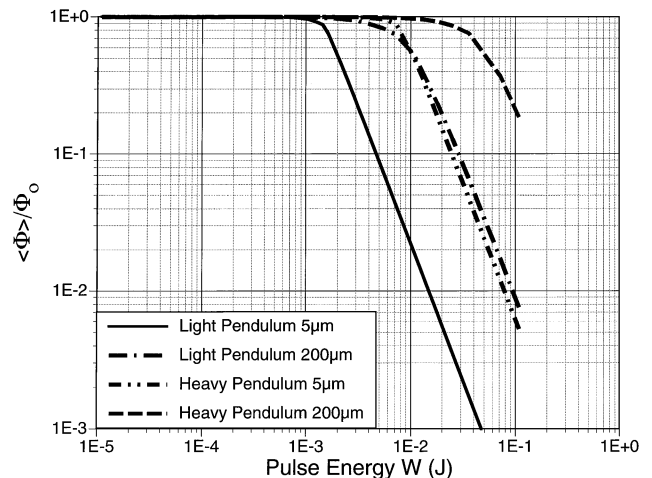


Fig. 7 Ratio of time average to peak fluence for light and heavy pendula vs pulsewidth, showing the effect of pendulum motion during the pulse [see Eq. (30) of text].

where

$$\begin{aligned} C &= \frac{4W_L f_\#^2}{\pi\tau}, & \gamma &= f_\#d_0, & \alpha &= f_\#d_1 \\ \beta &= \frac{\omega_0\theta_0 R}{2\tau}, & z &= \frac{\ddot{z}t^2}{2}, & \ddot{z} &= \frac{\omega_0\theta_0 R}{\tau} \end{aligned}$$

The integral (30) is tabulated,²⁶ and the result is

$$\begin{aligned} \langle\Phi\rangle &= \frac{C}{4\beta^2 q^3 \sin\psi} * \left\{ \sin\left(\frac{\psi}{2}\right) \ln \left[\frac{t^2 + 2qt \cos(\psi/2) + q^2}{t^2 - 2qt \cos(\psi/2) + q^2} \right] \right. \\ &\quad \left. + 2 \cos\left(\frac{\psi}{2}\right) \tan^{-1} \left[\frac{t^2 - q^2}{2qt \sin(\psi/2)} \right] \right\} \Big|_0^\tau \end{aligned} \quad (31)$$

with

$$q^2 = \frac{\sqrt{\alpha^2 + \gamma^2}}{\beta}, \quad \Psi = \cos^{-1} \left[\frac{-1}{\sqrt{1 + (\gamma/\alpha)^2}} \right] \quad (32)$$

Figure 7 shows how time-average fluence varies with pulse width using Eq. (30) and experimental parameters. The bottom line is that the heavy pendulum must be used for pulse energy $W > 1$ mJ (5- μm spot) or $W > 10$ mJ (200- μm spot). Even with the heavy pendulum and 200- μm focal spot size, results start losing their meaning because of varying spot size around 300 mJ. For this reason we have no data for higher energy.

Experimental Setup

The diffraction-limited beam from an SDL, Inc., XC30 single-mode research laser was sent through a vacuum chamber window and focused on the target using an axial gradient index lens (Lightpath Technologies, Inc.). This technology yields a relatively inexpensive simple-lens shape, which matches the optical performance of an aspheric (Figs. 8 and 9).

Transition to the vacuum laser momentum coupling regime will be essentially complete at 500 mtorr. That is, the residual gas will make little difference to C_m or I_{sp} at this pressure. We maintained chamber pressure less than 0.3 mtorr.

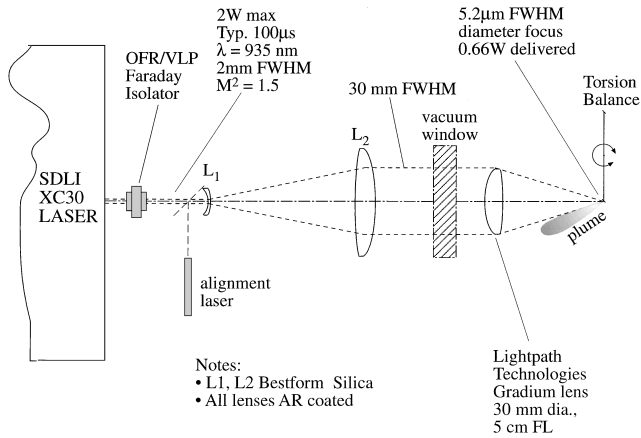


Fig. 8 Schematic of tabletop test setup. The window before the final focusing lens is a vacuum window. Target illumination $NA = 0.47$ and spot diameter $d_s = 5.2 \mu\text{m}$ full width at half-maximum (FWHM). The Faraday isolator prevents backreflections from interfering with single-mode operation of the laser. Beam quality $M^2 = 1.5$ is equivalent to a beam brightness of 80% of the theoretical maximum. Pressure in the chamber was typically 0.2 mtorr. No effort was made to attain high vacuum conditions. Pressures less than a few mtorr are sufficient to avoid interfering with plasma formation and expansion.

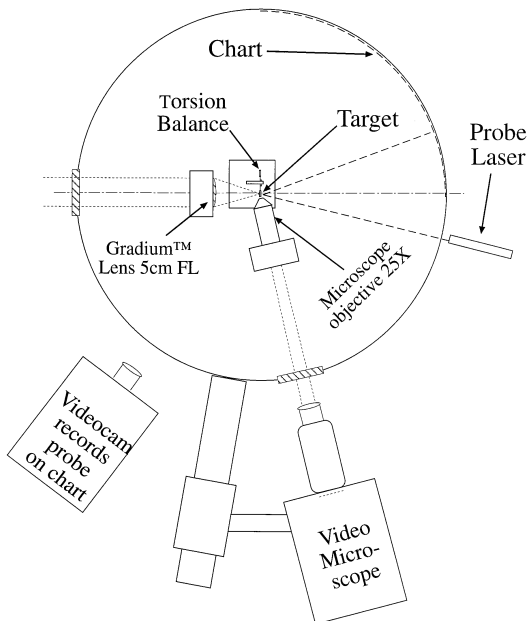


Fig. 9 Plan view of setup inside target chamber. Target position is measured to within $\pm 3 \mu\text{m}$ using the video microscope. Spot size is determined by analyzing the illumination distribution scattered from a fixed planar target, which is substituted for the target. The videocam views the chart through a bell jar, which sits on top of spool shown. Precise axial motion of the beam waist (best focus) with respect to the target was achieved with a 20:1 “leverage” by moving external lens L2 (see Fig. 8) on a translation stage.

Pendulum deflection was determined by reading the maximum deflection θ_b of the probe beam reflected from the mirror at the center of the pendulum onto a ruled chart attached to the inside of the vacuum chamber. This reading was recorded by the video camera/recorder indicated in Fig. 9, and the recordings analyzed frame by frame for maximum deflection at the conclusion of an experiment series. Because the chart was cylindrical in shape, no additional error was associated with reading large vs small deflections. Resolution of the technique was 0.1 mm at 23.5-cm radius, corresponding to 210 μrad of pendulum motion or, for the light pendulum, 1.45 nN/s. A few measurements were made using a 3.4-m optical lever arm (and a chart located outside the chamber), enabling about seven times higher resolution for very small deflections. These gave the 200 pN-s minimum resolution figure given in Table 2.

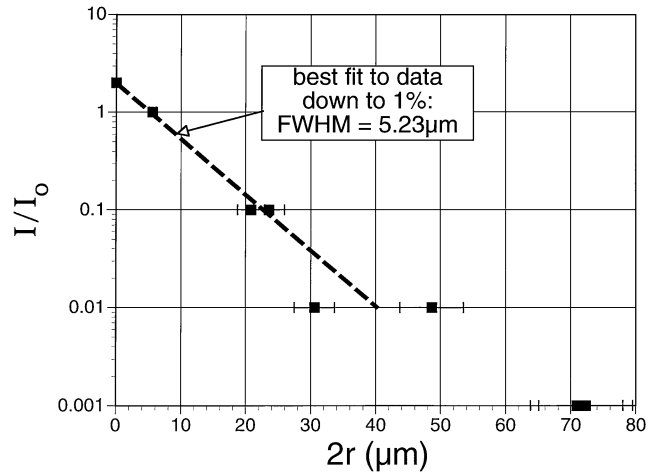


Fig. 10 Best fit to top 99% of intensity distribution gives spot diameter $d_s = 5.2 \mu\text{m} \pm 10\%$ FWHM.

The minimum impulse we observed in any of our measurements was 400 ± 200 pN-s. A typical measurement series covered 1–15 μN -s.

The laser was usually operated at 50% of maximum output (1 W) for long life and constant output. Attenuation through the Faraday rotator, lenses, and windows gave 0.66 W incident on the target with 1-W laser output. Figure 10 demonstrates that spot diameter on target was $5 \mu\text{m} \pm 10\%$.

Results

A total of 106 single-pulse data sets were taken using the single-mode research laser on materials ranging from black PVC film to black ink on paper, in both R and T illumination modes.

About half of these data were taken in R mode with the jet on the same side of the target as the incident light. Other data are instead taken in T mode, the laser beam passing through a transparent, highly damage-resistant substrate film to blow off an absorbing coating on the opposite side. This mode has two important features relative to the R mode: 1) vapor blown off the target cannot cloud the focusing optics and 2) the construction of the thruster itself is simplified.

Optics contamination was a minor problem in the approximately 2000 individual shots taken in our research program. However, for the much longer exposure expected in the prototype thruster’s lifetime keeping the optics clear will require more effort. T-mode illumination is an effort to address this problem.

We mainly used polyethylterephthalate (PET) and Kapton™ polyimide resin film, 100–125 μm thick, for T-mode measurements.

Black PVC film gave the best consistent results for C_m and I_{sp} of any ablatant we tested. Black polymethylmethacrylate (PMMA) also gave good results but did so less consistently and was more difficult to handle.

Figure 11 shows a typical range of target ablation spots in PVC film. The majority of our single-pulse data was taken with PVC films. Figures 12 and 13 show our R-mode PVC data for C_m and I_{sp} using 5- μm spot size. Figures 14 and 15 show T-mode PVC data for both 5- and 100- μm spot size. Scatter is discussed in the following section. Table 3 summarizes data for these and some additional materials. Perhaps most promising among these is the triazene “designer polymer” being developed for us by polymer chemists at the Paul Scherrer Institut.²⁷

Measurement Errors

Standard errors in measuring C_m were $\pm 10\%$ and in measuring $I_{sp} \pm 25\%$. For C_m these come from the combined uncertainty of measuring pulse energy and pendulum deflection and pendulum calibration error. The latter is $\pm 4\%$ (Table 2), and pendulum deflection error in the range of data reproduced here is $\pm 2\%$. The remainder of the error is caused by uncertainties in the laser calorimeter response.

For I_{sp} , determined from the product $C_m Q^*$, measurement uncertainties are those of C_m augmented by the larger uncertainties inherent in our measurement of excavated mass leading to Q^* .

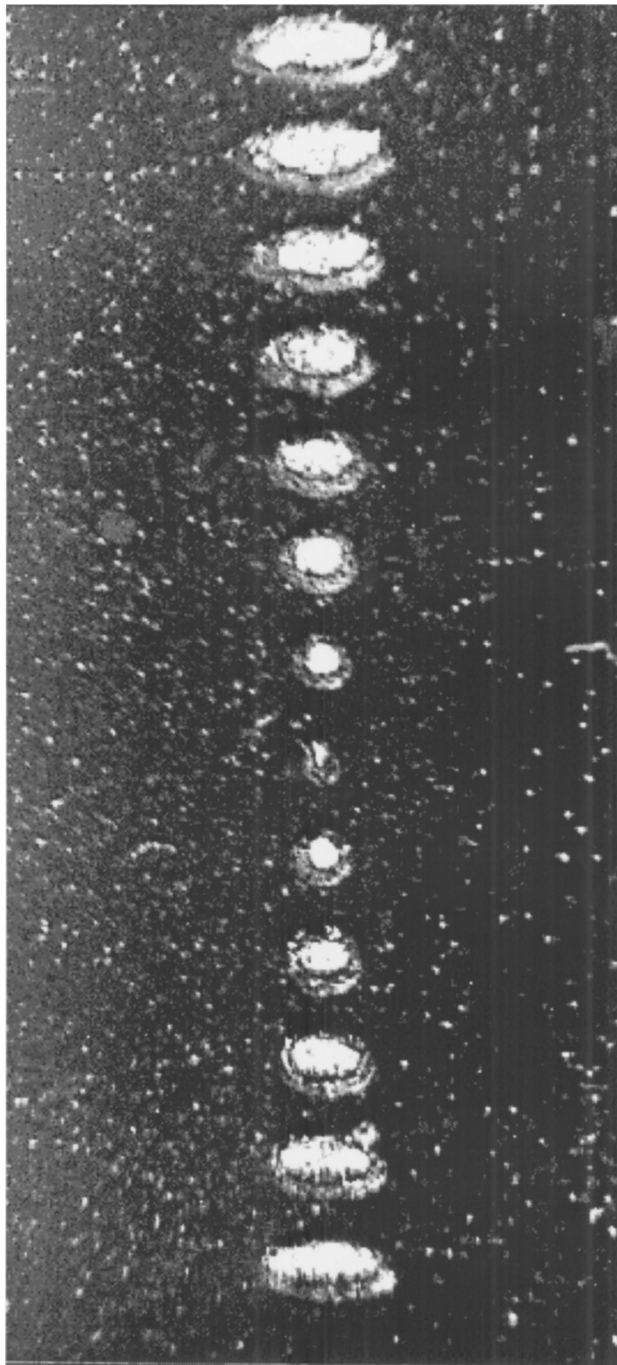


Fig. 11 Photomicrographs of single-pulse target burn spots taken while focusing the multimode diode laser range from $425 \times 170 \mu\text{m}$ (top) to $390 \times 125 \mu\text{m}$ (bottom), with best focus at center producing a $100 \times 25 \mu\text{m}$ ablation spot. The illumination distribution that produced this spot (image of diode output facet) is estimated to be $100 \times 5 \mu\text{m}$. High-divergence (“fast”) axis of laser is oriented horizontally. Absorbing film was $20 \mu\text{m}$ thick; substrate was $100 \mu\text{m}$ PET.

In all of the single-pulse measurements, ablated mass was on the order of nanograms, and so it was impossible to determine it by weighing the targets. Instead, it was necessary to determine Q^* by direct microscopic measurement of the excavated volume. Though we avoided assigning Q^* values when the character of the target ablation did not involve clean craters, some uncertainty in the results derives from qualitative judgment factors. This source of error will be eliminated when long-term continuous operational data from the prototype are available.

Discussion

Coupling coefficients measured on a planar surface, which is much larger than the illumination spot, will be enhanced (relative to

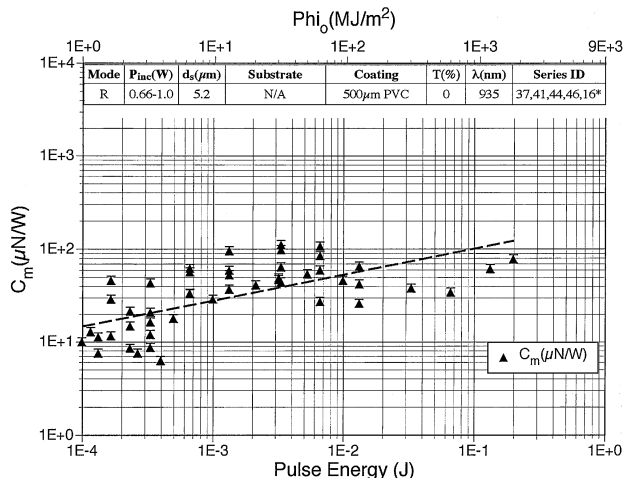


Fig. 12 Combined data from several measurement series showing coupling coefficient for black PVC film, R-mode, $5\text{-}\mu\text{m}$ -diam laser spot.

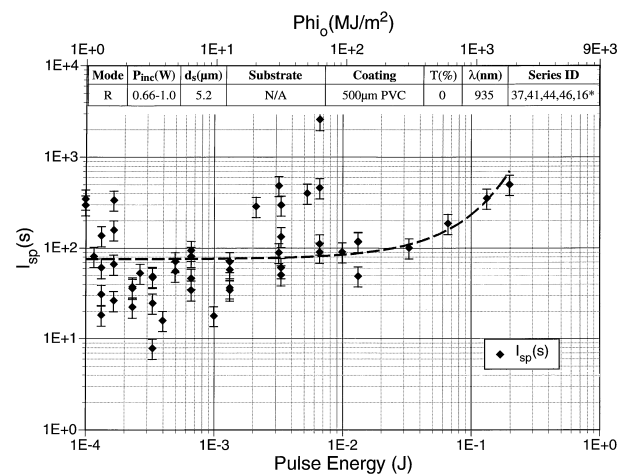


Fig. 13 Combined data from several experiments showing specific impulse, black PVC film, R mode, $5\text{-}\mu\text{m}$ illumination spot.

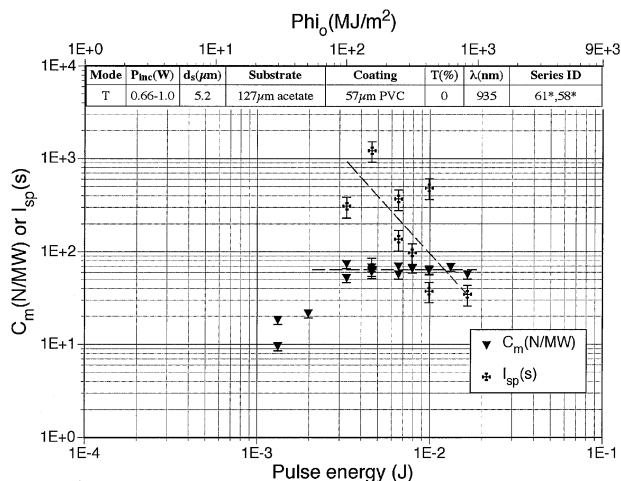


Fig. 14 Coupling coefficient and specific impulse measured with single pulses from the single-mode research laser focused to $5\text{-}\mu\text{m}$ spot diameter, on PVC/acetate target in T mode.

comparable literature values) by a large contribution from the initial blast wave as it spreads across this surface. Comparable standard data for carbon-bearing materials¹⁸ give $C_m = 45 \mu\text{N/W}$, about 40% of what we see.

Scatter in the C_m and I_{sp} data is not accounted for by the error bars associated with the measurement techniques. Scatter was observed to be larger with data taken at $5 \mu\text{m}$ than with $100\text{--}200\text{-}\mu\text{m}$ laser spot diameter. We believe the scatter is partly caused by spot-to-spot

Table 3 Single-pulse data summary

Ablatant (substrate) [data series]	Mode	$d_s, \mu\text{m}$	Peak of best-fit $C_m, \mu\text{N/W}$	Peak of best-fit I_{sp}, s
PVC [37, 41, 44, 46, 16*]	R	5	120	650
Printer's ink (paper) [4, 12, 30]	R	5	32	200
PVC (PET) [46*]	T	100	65	300
Scherrer triazene polymer (PET)[23*, 24*]	T	5	50	200
PVC (PET) [44*]	T	5	45	500

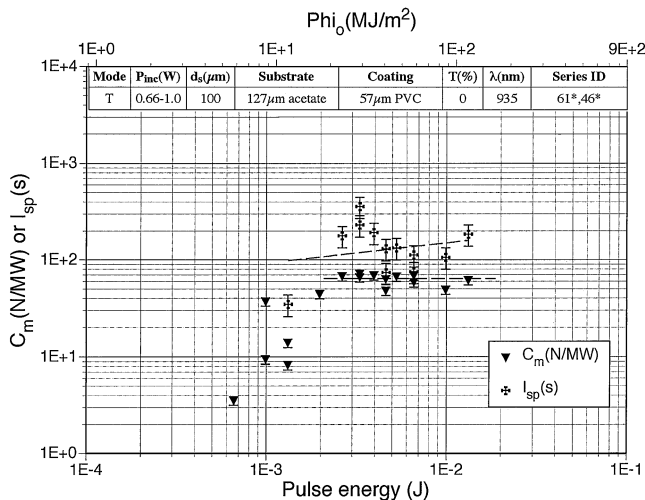


Fig. 15 Coupling coefficient and specific impulse measured with single pulses from the single-mode research laser on PVC/acetate target in T mode. Here, 100- μm spot diameter was used (compare Fig. 14). As expected, I_{sp} does not reach as large a maximum value.

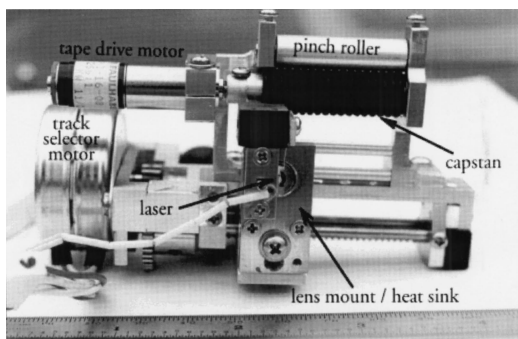


Fig. 16 LPT test assembly prior to insertion in vacuum chamber.

variations of the ablatant physical and chemical properties over a 5- μm scale, including granularity effects in the carbon doping material employed to achieve absorbance. These effects will always be more pronounced near ignition threshold (low fluence) than at maximum fluence in any set of data. More weight should be given to the high-fluence than the low-fluence data in any set.

R mode showed more scatter than T-mode data. We believe that interference of the ejecta with the incident beam might have been responsible. Target granularity is also an important contributing factor to data scatter in both modes.

The trend with R-mode data is for increased C_m with increased fluence, opposite to the trend with T-mode data. The main reason for this is that in R mode the available ablatant was infinite, practically speaking, whereas in T mode a fixed coating thickness was available for coupling to the laser beam. After the material is burned, further increases in fluence can only lead to lower C_m .

Table 3 shows that C_m is reduced by about a factor of two in T mode, but I_{sp} stays relatively high. One significant difference for this mode is that its performance is optimized for a relatively narrow pulse duration range. This is because the absorbing surface

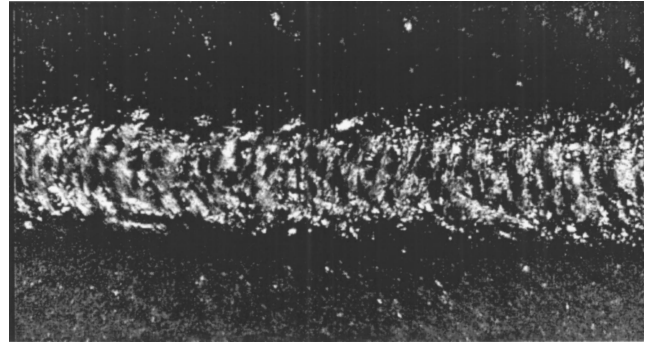


Fig. 17 Continuous track formed with the multimode laser at 0.4-W laser power is 250 μm wide. Target speed was 2.8 mm/s. Picture is of exit surface, front lit.

is heated first at the interface and rapidly blown off. It needs to be thin—not much thicker than one absorption depth; otherwise, most of the ejecta will not be heated, and I_{sp} will be low, even though C_m remains high. In contrast, in the reflection mode the absorbing surface can be arbitrarily thick and still achieve the same I_{sp} as the laser burns slowly through at the surface recession velocity of a few centimeter per second.

Prototype

We have mostly finished the impulse data, have selected a preliminary target material, and have done short continuous burns. The next step is development of a continuous thrust experiment, including a continuous loop tape drive, thrust stand, etc., followed by design and testing of a finished prototype configuration. Figure 16 shows construction details, and Fig. 17 shows a track obtained with the continuous thrust setup.

Conclusions

We demonstrated the feasibility of the laser microthruster concept. Impulse bits as small as 0.4 nN/s (40 $\mu\text{dyn-s}$) were measured during a 60- μs pulse. Maximum impulse with our 1-W laser during a 0.3-s pulse was 20 $\mu\text{N-s}$. The range between these extremes is nearly five orders of magnitude.

We measured specific impulse as large as 1000 s, 500 s being typical for pulses longer than 50 ms. Coupling coefficients were as large as 210 $\mu\text{N/W}$, 120 being typical. Exhaust velocity (determined from the product of C_m and Q^*) ranged up to 5 km/s.

We routinely created 5- μm laser spots on targets with low-spot-size jitter. We found spot sizes up to 200 μm useful to maximize coupling efficiency by avoiding target burnthrough for longer pulses, as well as to provide more spatially uniform target illumination. To measure such small impulses accurately, we created and accurately calibrated a highly sensitive microbalance. We have obtained a continuous track on our PVC ablatant in transmission mode using a 2-W multimode laser.

Appendix: Further Work

The largest continuous power available today from a high-brightness, single-facet diode laser is 4 W (SDLI 6380-A). At 3-mm/s target translation speed a 5 \times 100 μm image of this facet will offer an exposure time of 8.3 ms at a fluence of 65 MJ/m². From Fig. 2 this fluence is more than adequate for plasma formation. However, our codes predict that this fluence cannot achieve the ultimate potential of this technique as regards specific impulse. Passively Q-switched, repetitively pulsed, diode-pumped solid-state lasers that weigh only 15 g are now available in the 1-W average power range (Dunton, E., private communication, Litton-Airtron Corp., Los Angeles, June 2001). Nanosecond-duration pulses give 50-kW peak power, allowing us to access all materials and create temperatures high enough for very large I_{sp} (8000 s have been measured with nanosecond-duration laser pulses⁵).

Diode-pumped, glass fiber lasers offer an interesting alternative for achieving higher CW power with adequate brightness and small mass penalty.

We continue to explore R-mode illumination. The most encouraging results in the literature¹³ for forward-peaked ablation plumes have given a polar distribution $\propto \cos^{10} \theta$. We intend to measure the ablation polar distribution. We are planning experiments with a new optical design, which we believe can utilize this polar distribution without becoming contaminated during thruster lifetime.

We also continue to explore specially designed polymers for T-mode or R-mode operation. We believe these have tremendous potential for improving LPT performance.

Acknowledgments

This work was performed with the support of the U.S. Air Force Office of Scientific Research under STTR Phase I Contract F49620-98-C-0038 and STTR Phase II Contract F49620-00-C-0005. We gratefully acknowledge the assistance of Thomas Lippert and his team at the Paul Scherrer Institut, Zurich, in developing specially designed polymers for this work. We are also happy to acknowledge the tireless support to our work throughout this program provided by John Marquis, director of the Energy Conversion Research Laboratory at New Mexico Engineering Research Institute.

References

- ¹Lang, R., O'Brien, S., Schoenfelder, A., Hagberg, M., Demars, S., and Li, B., "High Power, High Brightness Diode Lasers," *1998 Diode Laser Technology Review*, U.S. Air Force Research Laboratory, AFRL/DELS, Kirtland AFB, NM, 1998.
- ²Phipps, C. R., and Dreyfus, R. W., "Laser Ablation and Plasma Formation," *Laser Microprobe Analysis*, edited by A. Vertes, R. Gijbels, and F. Adams, Wiley, New York, 1993, Chap. 4, pp. 369–431.
- ³Haglund, R. F., Jr., Ermer, D. R., Papantonakis, M. R., Park, H. K., and Yavas, O., "Phase Explosion and Ablation in Fused Silica Initiated by an Ultrashort-Pulse, Tunable Mid-Infrared Free-Electron Laser," *Proceedings of the International Symposium on High Power Laser Ablation 2000*, Vol. 4065, Society of Photo-Optical Instrumentation Engineers, Bellingham, WA, 2000, pp. 42–51.
- ⁴Phipps, C. R., Turner, T. P., Harrison, R. F., York, G. W., Osborne, W. Z., Anderson, G. K., Corlis, X. F., Haynes, L. C., Steele, H. S., Spicochi, K. C., and King, T. R., "Impulse Coupling to Targets in Vacuum by KrF, HF and CO₂ Lasers," *Journal of Applied Physics*, Vol. 64, No. 3, 1988, pp. 1083–1096.
- ⁵Phipps, C. R., and Michaelis, M. M., "Laser Impulse Space Propulsion," *Journal of Laser and Particle Beams*, Vol. 12, No. 1, 1994, pp. 23–54.
- ⁶Afanas'ev, Yu. V., Basov, N. G., Krokhin, O. N., Morachevskii, N. V., and Sklizkov, G. V., "Gas-Dynamic Process in Irradiation of Solids," *Soviet Physics-Technical Physics*, Vol. 14, No. 5, 1969, pp. 669–676.
- ⁷Apostol, I., Vatanov, V. A., Mikheilesku, I. N., Morzhan, I., Prokhorov, A. M., and Fedorov, V. B., "Recoil Impulse Received by Metal Targets as a Result of Interaction with Microsecond CO₂ Laser Radiation," *Soviet Journal of Quantum Electronics*, Vol. 6, 1976, pp. 1119, 1120.
- ⁸Augustoni, A. L., Ermer, P. G., Heckler, R. T., Kuwashima, G. R., McKay, J. A., and Rudder, R. R., "The Interaction of High Energy Single Pulse XeF Laser Radiation with Solid Targets," U.S. Air Force Research Lab., AFWL-TR-85-126, Kirtland AFB, NM, 1986.
- ⁹Combis, P., David, J., and Nierat, G., "Mesure des Effets Mécaniques dans les Expériences d'Interaction Laser-Matière à Eclairage Modéré," *Revue Scientifique et Technique de la Défense, CEL-Valenton No. 4*, Centre des Etudes Limeil-Valenton, Villeneuve-Saint-Georges, France, 1992, pp. 59–75.
- ¹⁰McKay, J. A., and Laufer, P. M., "Survey of Laser-Produced Pressure and Impulse Data," Physical Sciences, Inc., Final Rept. PSI-1012/TR-757, New England Business Center, Andover MA, 1987, pp. 1–236.
- ¹¹Duzy, C., Woodroffe, J. A., Hsia, J. C., and Ballantyne, A., "Interaction of a Pulsed XeF Laser with an Aluminum Surface," *Applied Physics Letters*, Vol. 37, No. 6, 1980, pp. 542–544.
- ¹²Gregg, D., and Thomas, S. J., "Momentum Transfer Produced by Focused Laser Giant Pulses," *Journal of Applied Physics*, Vol. 37, No. 7, 1966, pp. 2787–2789.
- ¹³Dreyfus, R. W., "Cu⁰, Cu⁺, and Cu₂ from Excimer-Ablated Copper," *Journal of Applied Physics*, Vol. 69, No. 3, 1991, pp. 1721–1729.
- ¹⁴Phipps, C. R., Harrison, R. F., Shimada, T., York, G. W., Turner, T. P., Corlis, X. F., Steele, H. S., Haynes, L. C., and King, T. R., "Enhanced Vacuum Laser Impulse Coupling by Volume Absorption at Infrared Wavelengths," *Laser and Particle Beams*, Vol. 8, 1990, pp. 281–297.
- ¹⁵Rosen, D. I., Nebolsine, P. E., and Wu, P. K. S., "Laser Impulse Applications Research," *Proceedings of the AIAA Conference on the Dynamics of High Power Lasers*, AIAA, New York, 1978, paper VI.
- ¹⁶Rosen, D. I., Hastings, D.E. and Weyl, G.M., "Coupling of Pulsed 0.35- μm Laser Radiation to Titanium Alloys," *Journal of Applied Physics*, Vol. 53, No. 8, 1982, pp. 5882–5890.
- ¹⁷Rosen, D. I., Mitteldorf, G., Kothandaraman, G., Pirri, A.N., and Pugh, E. R., "Coupling of Pulsed 0.35- μm Laser Radiation to Aluminum Alloys," *Journal of Applied Physics*, Vol. 53, No. 4, 1982, pp. 3190–3200.
- ¹⁸Rudder, R. R., U.S. Air Force Research Lab., AFWL-TR-74-100, Kirtland AFB, NM, 1974, pp. 189–198.
- ¹⁹Shui, V. H., Young, L. A., and Reilly, J. P., "Impulse Transfer from Pulsed CO₂ Laser Irradiation at Reduced Ambient Pressures," *AIAA Journal*, Vol. 16, 1978, pp. 649, 650.
- ²⁰Ursu, I., Apostol, I., Dinescu, M., Mihailescu, I. N., and Moldovan, M., "Plasma-Target Coupling in the Case of TEA-CO₂ Laser Produced Breakdown in Front of a Solid Target," *Optics Communications*, Vol. 39, 1981, pp. 180–185.
- ²¹Pucik, T., and Crawford, R. C., "Optical Laser Impulse Coupling Data Package," Logicon/R&D Associates, RDA Rept. 2.28.90, Los Angeles, 1990.
- ²²Weast, R. C. (ed.), *Handbook of Chemistry and Physics*, 58th ed., CRC Press, Cleveland, OH, 1978, pp. C-794, C-796, D-165, and E-10.
- ²³Eshbach, O. W. (ed.), *Handbook of Engineering Fundamentals*, 2nd ed., Wiley, New York, 1955.
- ²⁴Harper, C. A. (ed.), *Handbook of Plastics and Elastomers*, McGraw-Hill, New York, 1976, pp. 1–24 and 3–59.
- ²⁵Phipps, C. R., Reilly, J. P., and Campbell, J. W., "Optimum Parameters for Laser-Launching Objects into Low Earth Orbit," *Journal of Laser and Particle Beams*, Vol. 18, No. 4, 2000, pp. 661–695.
- ²⁶Gradshteyn, I. S., and Ryzhik, I. M., *Table of Integrals, Series and Products*, Academic Press, New York, 1965, Sec 2.161.1b, p. 67.
- ²⁷Lippert, T., David, C., Hauer, M., Wokaun, A., Robert, J., Nuyken, O., and Phipps, C. R., "Polymers for UV and Near-IR Irradiation," *Journal of Photochemistry Photobiology and Chemical Science* (to be published).

R. P. Lucht
Associate Editor